Cyclostationary Models of Solar Irradiance

Charlotte L. Haley and Mihai Anitescu
Department of Mathematics and Computer Science,
Argonne National Laboratory, 9700 S. Cass Ave, Argonne, IL 60439

Abstract
In this study we model solar irradiance at ground based sites in the continental US in order to predict into the future. The obvious nonstationary, non-Gaussian data have nightly zeros, or slightly negative values, producing dual frequency spectra with large values on the diagonals with offsets of 24 hours. Analysis of this particular covariance structure implies a a non-Gaussian process model with cyclostationary noise structure. Fitting stationary vs cyclostationary models reveals simpler and more accurate results are obtained using the cyclostationary framework.
Key Words: Time Series Analysis; Cyclostationary; Spectrum Analysis; Prediction & Forecasting

1 Introduction

Solar energy is one of the fastest growing energy sectors, accounting for 36% of all new electric generating capacity in the United States in the first three quarters of 2014. However both solar and wind inputs are relatively hard to predict due to large peaks and troughs in electricity generation resulting from local meteorological conditions. These swings in electricity generation can produce shortages and surges which have resulted in the need for frequent interventions from, e.g. coal power plants, which can be costly to operate at short notice and produce a lot of carbon. US net load data in states with large solar and wind power production, like California, have markedly different characteristics as a result of renewable inputs. Therefore it is of great interest to those attempting to forecast net load on the power grid to reliably predict the input from renewable sources. In this study, we consider the problem of short term prediction of solar irradiance, 2-8 hours in advance.

The problem of modeling solar irradiance was originally tackled using univariate time series data and simple autoregressive moving average (ARMA), k-nearest neighbor or artificial neural networks models [12, Ch. 15]. Usually this type of analysis is carried out with detrended and normalized data that is produced by division by a deterministic model such as Ineichen's model. With the incorporation of nonlocal information, short term forecasts can be significantly improved. Most of the uncertainty in solar irradiance is due to local cloud motion and dynamics, so the use of total sky imaging technology, see [4], produced data which allowed for the estimation of cloud motion vectors and hence the recovery of the solar irradiation when the cloud motion was projected into the future. To increase the forecasting window from minutes to hours, satellite data can be incorporated.

In this study, we seek to (i) further examine the covariance structure of such a nonstationary process, especially to (ii) estimate and characterize the particular diurnal changes in mean and variance of the series in the frequency domain, and finally to (iii) model the process using a very simple (a) stationary autoregressive and (b) cyclostationary process model and compare the (I) the residuals and (II) the result of a prediction based on both simple models. The main tool is the Loève spectrum, which allows for analysis general nonstationary processes.

1.1 Organization

This paper is organized into five sections, beginning in §2 with some necessary notation, tools and terminology. An introduction, literature review, and motivation are given in §3. Modeling, analysis, and prediction of multivariate ground data using an AR and VAR (periodically correlated AR) model are given in §4, along with discussion of the shortcomings of both approaches. We conclude in §5 with remarks and future work.

2 Notation and Terminology

We begin by recalling a few elementary definitions.

Definition 1 *A discrete-time* weakly stationary *process x_t has the following two properties*

$$\mathbf{E}\{x_t\} = \mu; \quad \mathbf{Cov}\{x_t, x_{t-\tau}\} = R(\tau). \tag{1}$$

That is, the expected value of the process does not depend on the time and the autocovariance function of the process is dependent only upon the lag.[1]

Definition 2 *A discrete process x_t is second order* cyclostationary *(or* periodically correlated*) with period $T > 1$ if T is the smallest integer such that the downsampled processes formed by extracting every T-th sample,*

$$\{\ldots, x_{t-T}, x_t, x_{t+T}, \ldots\}; \quad t = 0, \ldots, T-1, \tag{2}$$

are weakly stationary [10, 20, 9]. The mean, $m(t)$, of x_t is periodic, and the covariance $R(s,t)$ is doubly periodic *with period T, explicitly,*

$$\mathbf{E}\{x_t\} = m(t) = m(t+T); \quad \mathbf{Cov}\{x_s, x_t\} = R(s,t) = R(s+T, t+T) \tag{3}$$

Some autoregressive (AR) models are stationary.

Definition 3 *Autoregressive (AR) processes are generated by the following model equation [3]*

$$x_t = \sum_{j=1}^{p} \phi_j x_{t-j} + \varepsilon_t \tag{4}$$

where ε_t is white Gaussian noise process with zero mean, p is the model order, and $\{\phi_j\}_{j=1}^{p}$ are the model parameters.

AR models are stationary when the roots of their associated characteristic equation lie within the unit circle, see [3]. Parameter estimation and order selection for AR models is well known, usually involving the Yule-Walker equations, see e.g. [21, Ch 6] for these details.

Some periodic AR, or PAR, models fall within the class of cyclostationary processes.

Definition 4 *Periodic AR(p) models with period T, or PAR(p)-T models, can be expressed by the following model equation*

$$x_t = \sum_{i=1}^{p} \phi_i(t) x_{t-i} + \sigma(t)\zeta_t \tag{5}$$

where p is the model order and the coefficients $\phi_i(t)$ and $\sigma(t)$ are periodic with period T, i.e. $\phi_i(t) = \phi_i(t+T)$ for each i, $\sigma(t) = \sigma(t+T)$ are real and $\{\zeta_t : t \in \mathbb{Z}\}$ is white noise [10, p 233]. The last term, $\sigma(t)\zeta_t$, is called the shocks sequence *and the model in which $\sigma(t) = \sigma$ is called the constant-variance shocks (CVS) model.*

[1] The strong form of stationarity requires that the finite dimensional distributions of the process agree independently of the lag, see e.g. [19].

Consider the CVS PAR(1) model. When $\phi_1(t) = \phi < 1$, that is, $\phi(t)$ is constant, the CVS PAR(1) model reduces to a stationary AR(1) model. In order for the CVS PAR(1) model to be cyclostationary, the following condition must be satisfied

$$\prod_{t=0}^{T-1} \phi(t) < 1. \tag{6}$$

This condition ensures that the autocorrelation function, for $s > t$,

$$R(t,s) = \mathbf{E}\{x_t, x_s^*\} = \mathbf{E}\{x_t, x_t^*\} \prod_{k=t+1}^{s} \phi(k) \tag{7}$$

is bounded provided the variance function $R(t,t) = R(t+T, t+T) < \infty$.

The PAR(1) model can be written in the following vector format, [10, p 233],

$$\mathbf{x}_n = \phi_0^{-1}\phi_1 \mathbf{x}_{n-1} + \phi_0^{-1}\theta_0 \zeta_n \tag{8}$$

where

$$\mathbf{x}_n = \begin{bmatrix} x_{nT} \\ x_{nT-1} \\ \vdots \\ x_{nT-T+1} \end{bmatrix}; \quad \zeta_n = \begin{bmatrix} \zeta_{nT} \\ \zeta_{nT-1} \\ \vdots \\ \zeta_{nT-T+1} \end{bmatrix}; \quad \phi_1 = \begin{bmatrix} 0 & 0 & \dots & 0 \\ 0 & 0 & \dots & 0 \\ \vdots & \vdots & \ddots & \vdots \\ 0 & 0 & \dots & 0 \\ \phi(1) & 0 & \dots & 0 \end{bmatrix} \tag{9}$$

and

$$\phi_0 = \begin{bmatrix} 1 & -\phi(T) & 0 & \dots & 0 \\ 0 & 1 & -\phi(T-1) & \dots & 0 \\ \vdots & \vdots & \vdots & \ddots & \vdots \\ 0 & 0 & 0 & \dots & -\phi(2) \\ 0 & 0 & 0 & \dots & 1 \end{bmatrix}; \quad \theta_0 = \begin{bmatrix} 1 & -\sigma(T) & 0 & \dots & 0 \\ 0 & 1 & -\sigma(T-1) & \dots & 0 \\ \vdots & \vdots & \vdots & \ddots & \vdots \\ 0 & 0 & 0 & \dots & -\sigma(1) \\ 0 & 0 & 0 & \dots & 1 \end{bmatrix} \tag{10}$$

This model equation shows that PAR(1) processes can be expressed as vector autoregressive moving average, or VARMA, processes. This alternative vector formulation offers motivation for the use of vector-based models in §4 as general modeling tools, though there is no guarantee that the model actually fit is cyclostationary. There is a lot of literature on the subject of almost cyclostationary sequences (ACS) that is beyond the scope of this work [**?**]

The analogous *Yule-Walker* equations for the general PAR(p) processes are given in, e.g. [23, p 335-7] or [17]. They are derived by multiplying the expression (5) by x_s and taking the expected value. Here using $p = 1$ we obtain

$$R(t,t-s) + \phi(t)R(t-1,t-s) = \delta_s \sigma^2(t); \quad 0 \le t,s < T \tag{11}$$

where $\delta_s = 1$ when $s = 0$ and 0 otherwise. Recall that cyclostationary processes have autocorrelations $R(s,t)$ with the property (3) so $R(s,t)$'s indices can be written modulo T. As far as parameter estimation is concerned, substitution of different t,s in this equation leads to a system of equations that can be solved to find the coefficients $\phi_1(t) = \phi(t)$ and the sequence $\sigma(t)$.

2.1 Frequency-domain methods

Spectrum analysis applies strictly to stationary processes. Formally, the spectrum is defined as follows.

Definition 5 *The Cramér spectral representation theorem, [5, 21], states that for a stationary process $x(t)$, there exists a stationary, orthogonal increments process $dZ(f)$ such that*

$$x(t) = \int_{-1/2}^{1/2} e^{i2\pi ft} dZ(f) \tag{12}$$

When it exists, the spectrum of the process is then defined as $S(f) = \mathbf{E}\{|dZ(f)|^2\}$.

The spectrum also has the following convenient relation with the autocorrelation function of the process.

Theorem 1 *(Einstein-Wiener-Khintchine) The spectrum $S(f)$ and autocorrelation function $R(\tau)$ of a stationary, zero mean process x_t are related by a Fourier transform*

$$R(\tau) = \int_{-\frac{1}{2}}^{\frac{1}{2}} S(f) e^{-i2\pi ft} dt. \tag{13}$$

For example, it is easy to verify from the autocorrelation function of the stationary AR(p) process, that the spectrum of the stationary AR(p) process is [21, p. 168]

$$S(f) = \frac{\sigma_\varepsilon^2}{|1 - \sum_{j=1}^{p} \phi_j e^{-i2\pi fj}|^2}. \tag{14}$$

In practice, one estimates the spectrum of a process using a tapered, smoothed periodogram estimator, or better a multitaper estimator, as described in the appendix.

One method of determining frequency domain properties of nonstationary series is through the Loève spectrum. The existence of the Loève spectrum depends on harmonizability.

Definition 6 *Two sequences $x(t)$ and $y(t)$ are* jointly second order harmonizable *if, [16],*

$$\mathbf{E}\{x(t_1)y(t_2)\} = e^{i2\pi(\nu_1 t_1 \pm \nu_2 t_2)} d\tilde{\gamma}_{x,y}(\nu_1, \nu_2) \tag{15}$$

with $\tilde{\gamma}_{x,y}(\nu_1, \nu_2)$ spectral covariance of bounded variation

$$\int_{-\frac{1}{2}}^{\frac{1}{2}} \int_{-\frac{1}{2}}^{\frac{1}{2}} |d\tilde{\gamma}_{x,y}(\nu_1, \nu_2)| < \infty. \tag{16}$$

Under harmonizability, we have

$$x(t) = \int_{-\frac{1}{2}}^{\frac{1}{2}} e^{i2\pi\nu t} d\chi_x(\nu); \qquad y(t) = \int_{-\frac{1}{2}}^{\frac{1}{2}} e^{i2\pi\nu t} d\chi_y(\nu) \tag{17}$$

and we write $d\chi_x(\nu) = X(\nu)d\nu$ where

$$X(\nu) = \sum_{t\in\mathbb{Z}} x(t) e^{-i2\pi\nu t}, \text{ and } Y(\nu) = \sum_{t\in\mathbb{Z}} y(t) e^{-i2\pi\nu t}. \tag{18}$$

Definition 7 *The* Loève dual frequency cross spectrum*, sometimes Loève bifrequency cross spectrum or simply Loève spectrum, is defined as [20, p 187] [27, 15, p. 7]*

$$\tilde{S}_x(\nu_1, \nu_2) = \mathbf{E}\{X(\nu_1) Y^{(*)}(\nu_2)\} \tag{19}$$

and in the sense of distributions

$$d\tilde{\gamma}_{x,y}(\nu_1, \nu_2) = \mathbf{E}\{X(\nu_1) Y^{(*)}(\nu_2)\} d\nu_1 d\nu_2 \tag{20}$$

Note that the Loève spectrum can be computed using either (a) two different series $x(t)$, $y(t)$ at different frequencies, (where it is called a *cross spectrum* when unclear from the context) which allows one to examine common frequency components which contribute to the variance or (b) the same sequence $x(t)$ (where it is called an *autospectrum*) which allows for analysis of the nonstationary properties of the signal across frequency. A particularly useful normalized form of the Loève spectrum, looking ahead to Eqn. (33) is the Loève coherence. We consider mainly autospectra or autocoherences in this paper but [18] shows some examples of Loève cross spectra.

The Loève spectrum of a PAR(1) model is, Def. 4,

$$\tilde{S}_x(\nu_1,\nu_2) = \sum_{s,t} R(s,t) e^{-i2\pi(t\nu_1 - s\nu_2)} = \sum_{s,t} R(t,t) \prod_{k=t+1}^{s} \phi(k) e^{-i2\pi(t\nu_1 - s\nu_2)} \tag{21}$$

but can also be written in terms of the matrices using expression (8), in the following way

$$\mathbf{f}(\lambda) = \phi(e^{-i\lambda})^{-1} \phi_0^{-1} \theta_0 \theta_0^* [\phi_0^{-1}]^* [\phi(e^{-i\lambda})^{-1}]^* \tag{22}$$

where $\phi(z) = \mathbf{I}_{T\times T} - \phi_0^{-1}\phi_1 z$. Where in this expression, the Loève spectrum is written as a frequency-dependent vector.

An analogous (nonstationary) form of the Einstein-Wiener-Khintchine theorem, Thm. 1, sheds light on the interpretation of the Loève spectrum. If one takes the Fourier transform of the correlation function of two processes $x(t)$ and $y(t)$, denoted $R(t_1,t_2)$, and Fourier transforms the result, one obtains the *dual-frequency cross-spectrum* $\gamma_{x,y}(f_1,f_2)$

$$R(t_1,t_2) = \mathbf{Cov}\{x(t_1), y^*(t_2)\} = \int_{-\frac{1}{2}}^{\frac{1}{2}} \int_{-\frac{1}{2}}^{\frac{1}{2}} \gamma_{x,y}(f_1,f_2) e^{i2\pi(t_1 f_1 - t_2 f_2)} df_1 df_2 \tag{23}$$

The Loève spectrum has two frequency indices which correspond, by way of the Fourier transform, with the two temporal indices. The dual frequency spectrum can be converted to a dual frequency magnitude squared coherence (MSC) by normalizing

$$c_{x,y}(f_1,f_2) = \frac{\gamma_{x,y}(f_1,f_2)}{\sqrt{S_x(f_1) S_y(f_2)}} \tag{24}$$

where $S_x(f) = \gamma_{x,x}(f,f)$ is the (auto)spectrum of the process $x(t)$ and $c_{x,x}(f_1,f_2)$ is the autocoherence.

In practice one can compute the Loève spectrum using the multitaper approach described in [27], and as described in the appendix. Here, exclusively multitaper estimates are used because of their superior statistical properties, see e.g. [21, 25, 28].

When interpreting the Loève spectrum, note that when the series is stationary, the Loève spectrum is nonzero only on the diagonal. Any significant off-diagonal frequency pairs should be examined carefully as they reflect frequencies that work coherently [28]. Some simple examples of Loève spectra computed using seismic data are given in [18]. It is worth noting that the support of any cyclostationary process in terms of Loève spectra is a set of diagonal lines (see [11, p 330]) separated in frequency with (angular) spacing $2\pi/T$. This is shown in Fig. 1 to come.

Example 1 *Consider the stationary AR(2) model given by*

$$x_t = 0.8x_{t-1} - 0.2x_{t-2} + 0.2\zeta_t; \tag{25}$$

where ζ_t is a white noise signal with zero mean and unit variance. The Loève spectrum in Fig. 1a shows no significant off-diagonal elements.

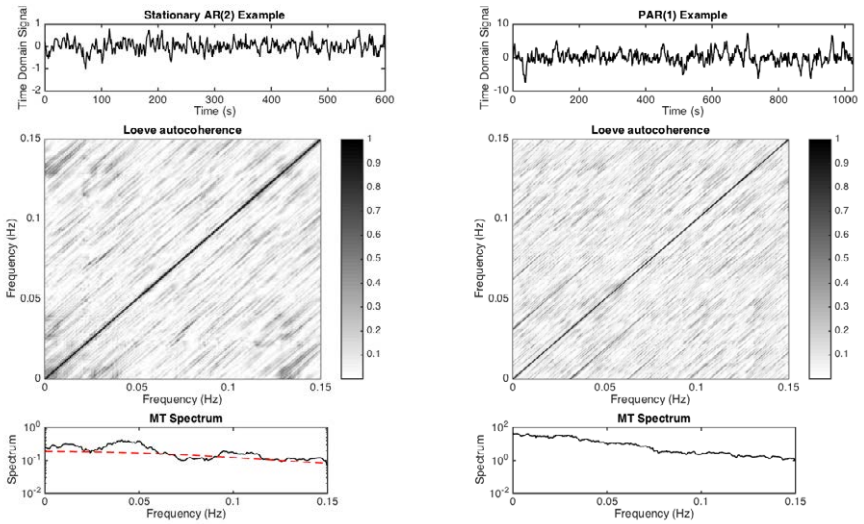

(a) (b)

Figure 1: Panels (a) show a 1024 point sample of an AR(2) process given in (25) in the time domain (top plot), a portion of the Loève (middle plot) and multitaper spectra ($NW = 6.5, K = 12$; bottom plot). The theoretical AR(2) spectrum is given by the dashed line in the bottom panel. Panels (b) show an example of a 1024 point simulated PAR(1) model, Eqn. (26). Note the prominent off-diagonal streaks in the Loève autocoherence due to cyclostationarity; in general the support of a cyclostationary process lies on diagonals in dual frequency space.

Example 2 *Following the example in [10, p 38-9] of PAR(1), Eqn* (5)*, the signal is constructed using*

$$\phi_1(t) = 0.6 + 0.4\cos 2\pi t/T \tag{26}$$

and constant shocks. The Loève spectrum is in the right panel of Fig. 1.

For additional examples of Loève spectra, consult [20, p 247-257] for cross-correlations or [18] for the multitaper Loève auto spectrum.

3 Motivation & Observational Data Analysis

3.1 Ground data

Data from 7 stations across the continental US in the NOAA Surface Radiation Budget Monitoring (SURFRAD) network can be obtained from `http://www.esrl.noaa.gov/gmd/grad/surfrad/overview.html`. The SURFRAD network was established in 1993 and provides, among other data products, downwelling solar irradiance data sampled at 3-minutes (1-minute sampling was introduced in the early 2000's). Bondville, IL data is mainly used in this study.

3.2 Observational Data Analysis

Solar irradiance varies by 2-3W/m^2 with the 11-year solar cycle, as measured from space [13, see Fig. 1]. Additionally, both from the spectrum, and from individual box plots, see Fig. 2, it is clear that these data have seasonally varying mean and variance.

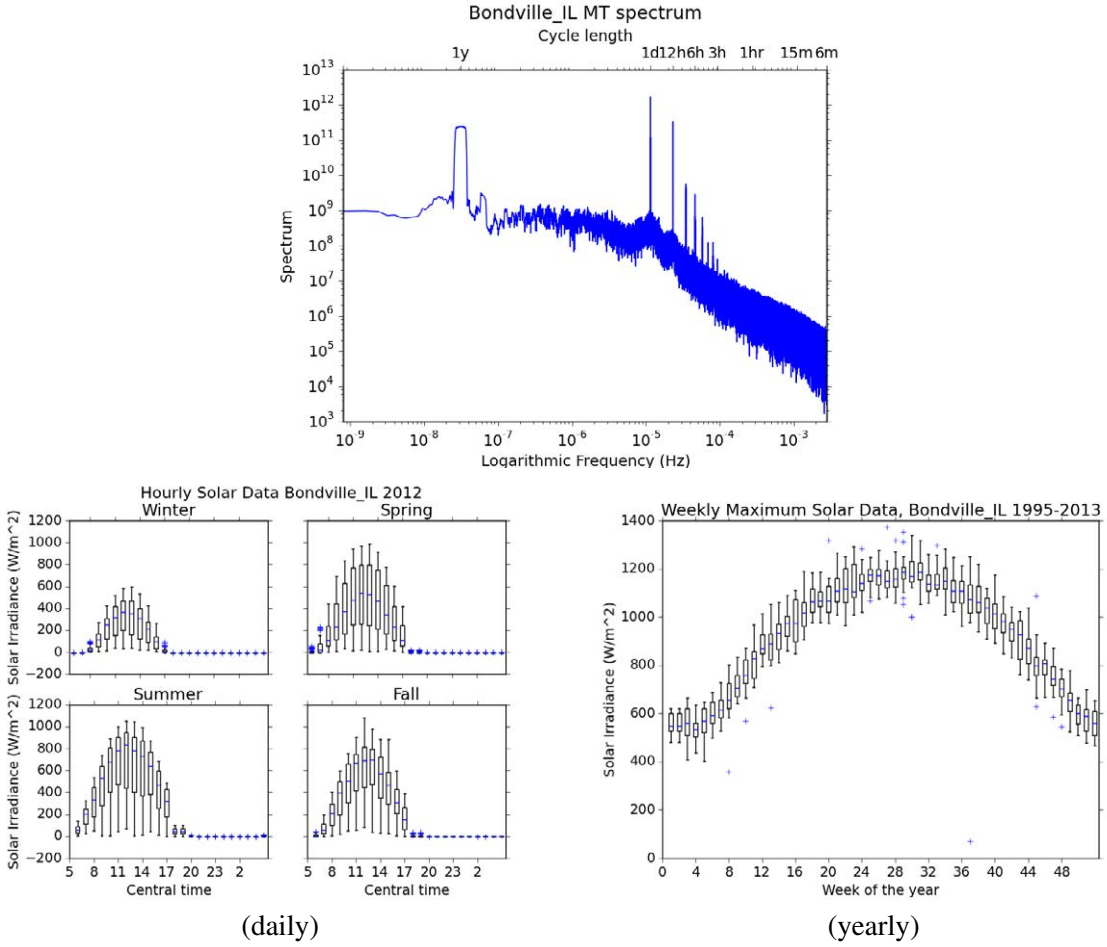

(daily) (yearly)

Figure 2: The top panel shows a multitaper ($NW = 4, K = 6$) spectrum calculated from Bondville IL data with 3-minute sampling. These data clearly contain a peak at one year, followed by daily components and harmonics thereof. The bottom left panel, labeled daily, shows boxplots of solar irradiance from Bondville, IL from Nov 7, 2012 to Nov 6, 2013 by hour of the day and by season, where seasons here have been centered on the winter solstice. The changing length of the day and the changing seasonal amplitude are prominent. In the bottom right panel, labeled yearly, the entire Bondville data have been used (1995-2014), and the maximum of the data in each weeklong block has been selected (week 0 being the week of January 1). These plots show the strength of the yearly modulation as well as the changes in variance throughout the daily cycle.

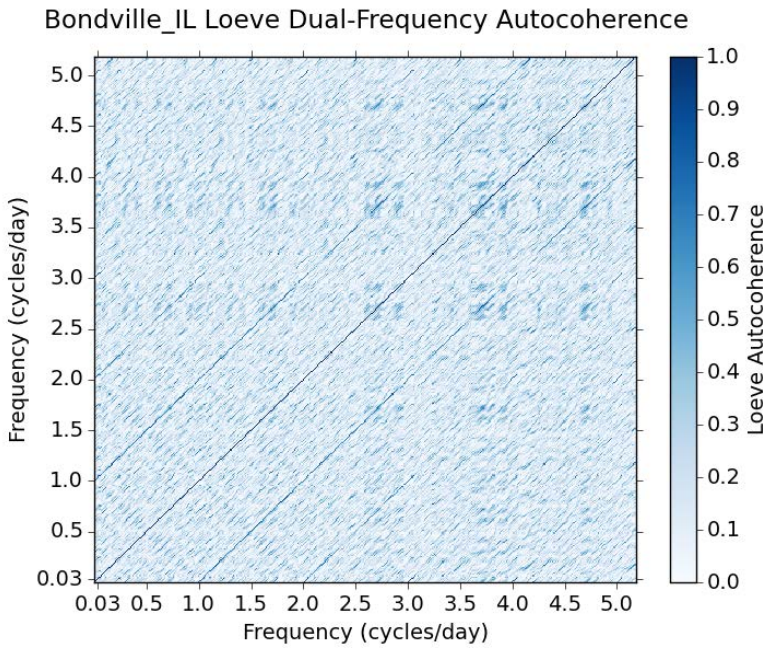

Figure 3: The Loève dual frequency (normalized) coherence generated from 2048 hours (85 days) of data from Bondville, Illinois beginning 4pm Sept 26, 2013 with hourly sampling (this results in Rayleigh resolution $\mathscr{R} = 64$nHz, and multitaper bandwidth $W = 257$nHz. There are prominent diagonal lines with one day spacing, c.f. right panel of Fig. 1.

It is important to stress that though the spectrum was shown in Fig. 2, to identify periodic components and their harmonics in these data, the assumption of additive harmonic components is overly simplistic. The Loève autocoherence, Eqn. 33, can be used to quantify nonlinear and nonstationary frequency domain relationships see [27, 28].

The main feature which can be discerned from the Bondville, IL solar irradiance Loève autocoherence in Fig. 3 is that there are distinct diagonal bands in frequency with separation 11.57μHz or 24 hours (multitaper parameters were chosen as $NW = 4, K = 6$ here). This indicates that there are strong correlations at all frequencies between the data and itself shifted one day, two days, and at some frequencies three days ahead. One also notices a peculiar "quilted" appearance to this Loève autocoherence due to normalization by the spectrum (Fig. 2 top), where the patches have side length about 11.57μHz.The quilted appearance can also be due to leaked discrete atoms contributed by a periodic mean, e.g. [10, p 175].

The difficulty in model selection for cyclostationary processes is exacerbated by the difficulty in removing trends. Over long time scales, any nonstationary model used to represent solar irradiance will also have diagonals with line components near the yearly and 11-year components. The difficulty in fitting line components like those seen in the bottom right panel of Fig. 3 using a simple AR model, without significant model complexity (high model order p), results in overly smooth parametric Loève spectra, which do not capture periodic components. These trends have to be estimated and removed in another way.

4 Time Series Models

In this section, we fit simple AR and nonstationary models to these data, and we compare the stationary approach to the nonstationary approach, contrasting the parametric spectra we get with the nonparametric estimates, as well as comparing trends in the residuals and the result of prediction using both of the models.

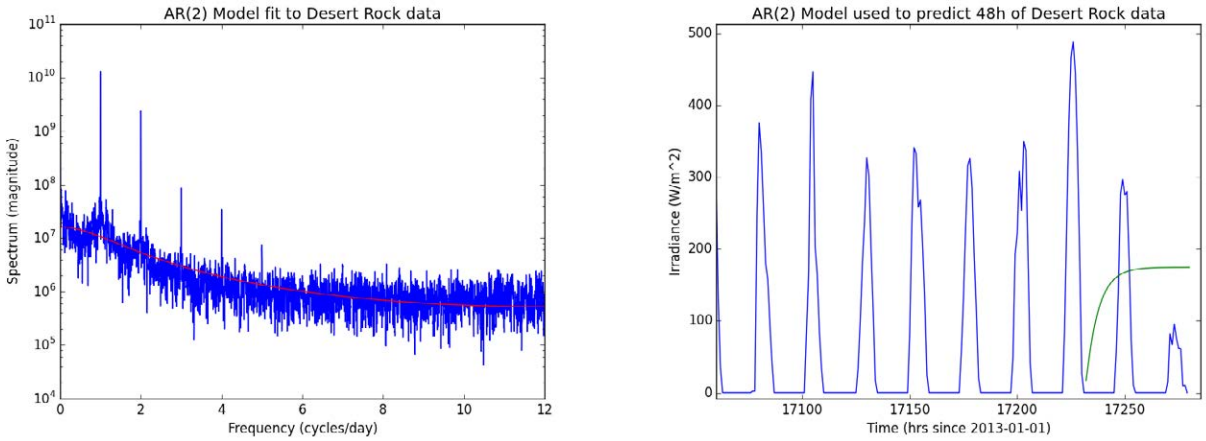

Figure 4: An AR(2) model is fit to the Desert Rock Data in the left panel. The red curve (overlaid) is the parametric spectrum, while the blue line shows the original nonparametric MT spectrum estimate. The coefficients given by the optimization procedure give a nonstationary model fit, that is, the roots of the characteristic equation lie outside the unit circle. The right panel shows the result of a prediction based on this covariance structure. Since the fitted model is nonstationarity, the prediction is not valid and the model gives an erroneous result.

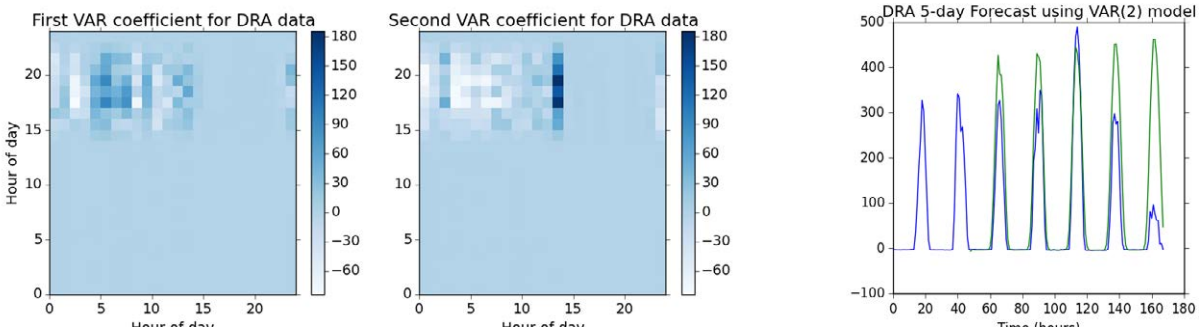

Figure 5: Steps of the VAR(2) model fitting (left and center plots) and the result of a 5d prediction (right plot) on the Desert Rock Data (prediction in green, data in blue).

In this section, hourly data is used for computational simplicity.

4.1 Stationary Models

Using the Python `statsmodels` package version 0.6.1, an AR(2) model was fit to these data. Fig. 4 shows the (standard) graphical process of model fitting. AR parameters were chosen as $[\mu, \phi_1, \phi_2] = [$ 172.48190203 1.05768942 -0.18225387] ,following the notation of Eqns (1) and (4). The fitted model is nonstationary, having roots for its characteristic equation outside the unit circle, see e.g. [3]. The Durbin-Watson test statistic for serial correlation was reported as 2.11, indicating slightly negative serial correlation.

The unfortunate consequence of a prediction based on an AR model with coefficients leading to a non-stationary model is that it produces nonsense, see the right panel of Fig. 4.

4.2 Cyclostationary Models

Motivated by the vector based implementation, Eqn. (8), of the PAR(1) model defined in Def. 4 one can use a vector based approach. A vector-based autoregression, or VAR(p), model has model equation, see [10, p 233-4]

$$\begin{bmatrix} x_t \\ x_{t+1} \\ \vdots \\ x_{t+T-1} \end{bmatrix} = \sum_{i=1}^{p} \begin{bmatrix} A^{(i)}_{0,0} & A^{(i)}_{0,1} & \dots & A^{(i)}_{0,T-1} \\ A^{(i)}_{1,0} & A^{(i)}_{1,1} & \dots & A^{(i)}_{1,T-1} \\ \vdots & \vdots & & \vdots \\ A^{(i)}_{T-1,0} & A^{(i)}_{T-1,1} & \dots & A^{(i)}_{T-1,T-1} \end{bmatrix} \begin{bmatrix} x_{t-iT} \\ x_{t+1-iT} \\ \vdots \\ x_{t-1+iT} \end{bmatrix} + \begin{bmatrix} \zeta_t \\ \zeta_{t+1} \\ \vdots \\ \zeta_{t+T-1} \end{bmatrix}. \tag{27}$$

where we have chosen T as the (known) cyclostationary period. If the process is cyclostationary with period T, then the vector process is stationary. VAR models can also be fitted using Python `statsmodels`, see Fig. 5. As can be seen from Eqns (8), the vector ARMA model contains the PAR(1) model. Fig. 5 shows the estimated coefficient matrices for a VAR(2) model fit to the solar data and the result of an example five day prediction.

The results of prediction using the two simple models are given in the right panels of Figs. 4 and 5. The conclusion that we come to with the stationary AR model is that it is entirely inappropriate for the data at hand. The VAR(2) model does much better in reproducing the daily peak, though the daily maximum in the forecast appears to be increasing.

Fig. 6 shows the ordinary autocorrelation functions, (one frequency) spectrum, and histograms of the residuals for both types of models. It is clear from left panel of Fig. 6 that there is periodicity in the autocorrelation function after the AR(2) model is removed. The residuals from the VAR(2) model do not have this feature, though they don't damp sharply to zero, and the ordinary spectrum retains a slight redshift.

It turns out that this can be removed by a combination VAR(2) & AR(2) model fit, see panel (c) of Fig. 6. The embedded model autocovariances damp quickly to zero, the spectrum appears nearly white, and the histogram of the residuals appears to have much lighter tails than the other two models.

5 Conclusions

5.1 Summary

We have gathered evidence for the use of cylostationary covariance structure on the solar irradiance data. We have used this to generate parametric models based on the assumption of (a) stationarity and (b) cyclostationarity, fitted the models, examined the residuals, and used both methods for prediction. We found that the cyclostationary model, however more like the nonparametric Loève spectrum, still does not capture the complexity of the overall process, while a combination of the two methods appears to whiten the spectral characteristics in the residual.

5.2 Discussion

In summary, this study shows the utility of a cyclostationary covariance structure in modeling solar irradiance. The study of cyclostationary signal processing has been a major topic of discussion for over 50 years [6]. A number of books [10, 20, 7] have been written as well as review articles [9] and workshops [8] on the subject. Here cyclostationary structure arises in a particularly important natural context.

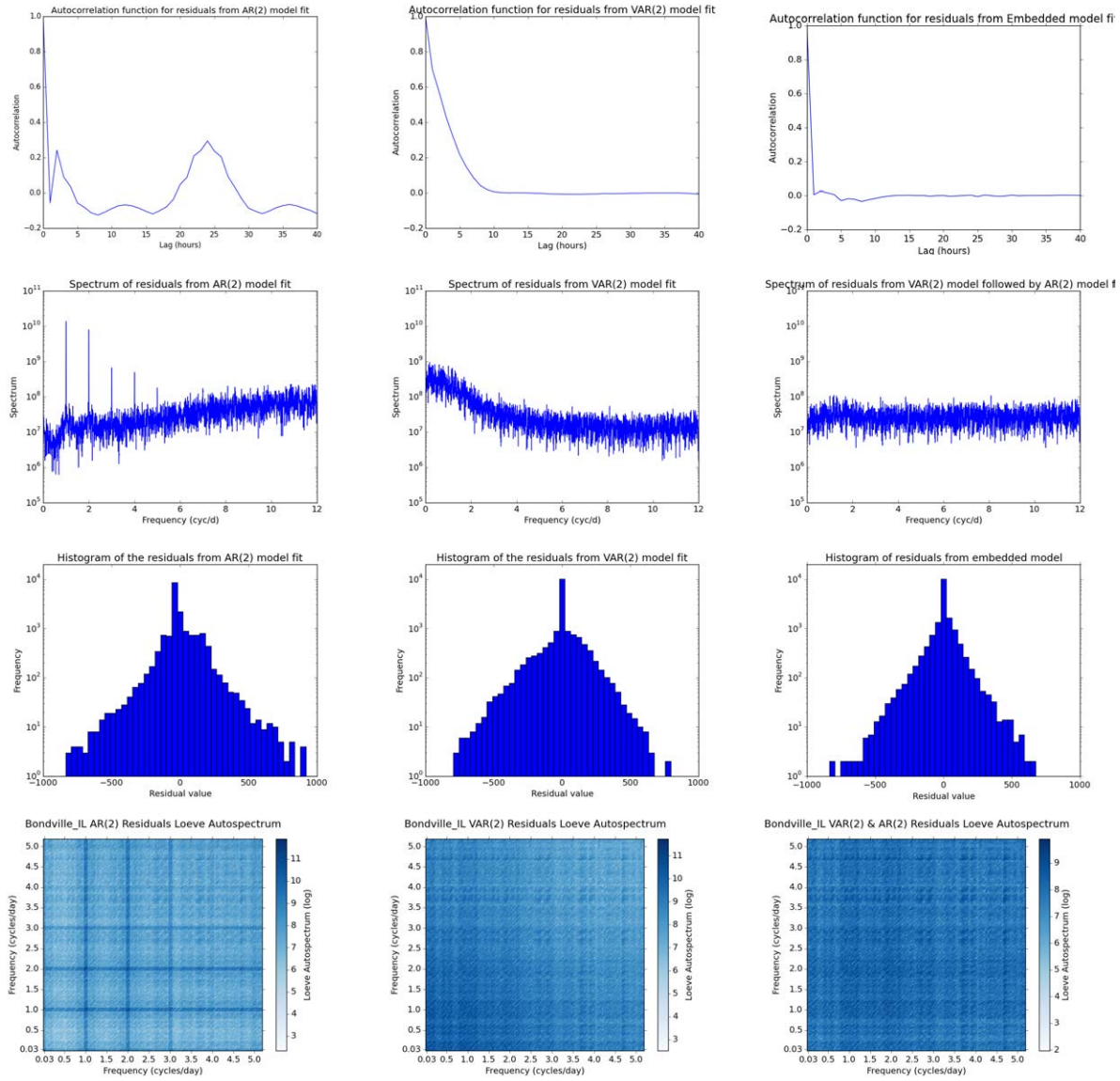

(a) (b) (c)

Figure 6: Autocorrelation functions (top) for the AR(2) model (a), the VAR(2) model (b), and the VAR(2) followed by AR(2) model (c) the spectra, histograms of the residuals, and the Loève spectra (bottom). . Loève spectra are calculated with 2048 hours of data for direct comparison with Fig. 3, however these figures are not normalized and are squared versions of Eqn. (23). The bottom right Loève spectrum, corresponding to the embedded VAR(2) and AR(2) models combined amount to a much whiter residual. Note different color scales.f

5.3 Data Sources

Downwelling global solar data is available from NOAA via ftp `ftp://aftp.cmdl.noaa.gov/data/radiation/surfrad/`.

Energy facts were obtained from the US Energy Information Administration Electricity data browser, Solar Energy Industries Association 2014 Fact sheet and the Institute for Energy research.

6 Appendix: Multitaper calculation of Loève Spectrum

General overviews of spectrum analysis are available in [2, 1]. The multitaper approach to spectrum estimation seeks to control the variance of the usual periodogram spectrum estimate by averaging K independent estimates of the spectrum which in turn are obtained by estimating the spectrum using K different orthogonal tapers. A good choice for the tapers are the Slepian sequences, which are concentrated in a given bandwidth in frequency and are near zero elsewhere, so they control bias by limiting leakage from faraway frequencies. By extension of multitaper spectrum estimation, one can use the multitaper approach to computing the Loève spectrum. This section contains a brief overview of this technique.

Slepian Sequences

The multitaper method of spectrum estimation makes use of the discrete prolate spheroidal, dpss or *Slepian* sequences, $\{v_n^{(k)}(N,W)\}_{k,n=0}^{N-1}$, which form a set of K length-N, orthogonal sequences $\mathscr{L}^2$-optimally concentrated on the band $(-W,W)$, $W < 1/2$ in frequency [24]. They satisfy the eigenvalue equation

$$\sum_{m=0}^{N-1} \frac{\sin 2\pi W(n-m)}{\pi(n-m)} v_m^{(k)}(N,W) = \lambda_k(N,W) \cdot v_n^{(k)}(N,W) \tag{28}$$

where the eigenvalue $\lambda_k(N,W)$ also denotes the fraction of energy in the band $(-W,W)$, and the index k sorts the sequences in descending order of energy concentration, $1 > \lambda_0 > \lambda_1 > \ldots > \lambda_{N-1} > 0$. The first $K \approx 2NW$ of the λ_k's are close to one, while the others rapidly drop to zero. We will drop the dependency on (N,W) in the rest of this appendix. When using a multitaper spectrum, it is important to quote the bandwidth parameter W which is often chosen as a function of the time-bandwidth product NW.

Solving the eigenvalue problem to get the dpss's is nontrivial, but there is an alternate formulation using a tridiagonal matrix which is computationally tractable [26]. See [22], for example, for an implementation in Fortran.

Multitaper Spectrum Computation

The multitaper spectrum is a weighted average of magnitude squared Fourier transformed tapered data sequences. Denoting the *eigencoefficients* as

$$y^{(k)}(f) = \sum_{t=0}^{N-1} x_t v_t^{(k)} e^{-i2\pi ft}, \tag{29}$$

and the *eigenspectra* as

$$\hat{S}^{(k)}(f) = |y^{(k)}(f)|^2, \tag{30}$$

the multitaper spectrum estimate is constructed as the following weighted average

$$\hat{S}(f) = \frac{\sum_{k=0}^{K-1} d_k^2(f)\hat{S}^{(k)}(f)}{\sum_{k=0}^{K-1} d_k^2(f)} \tag{31}$$

where the optimum frequency-dependent weights, $d_k(f)$, are determined using an adaptive scheme, see [25] §V. One can obtain a basic spectrum estimate using $d_k(f) = 1/\sqrt{K}$. The multitaper offers, among numerous advantages listed in, say [21], control of variance through averaging independent estimates and control of bias using approximately bandlimited tapers.

Multitaper spectrum estimation has been implemented in Python using the `pymutt` package [14].

6.1 Loève Spectrum

The multitaper estimate of the Loève spectrum is computed as follows [18]. If $x_1(f),\ldots,x_K(f)$ and $y_1(f),\ldots,y_K(f)$ are eigencoefficients of two series x_t and y_t with set bandwidth W and number of Slepian tapers K, then the Loève spectrum is estimated simply as [28]

$$\hat{S}_{x,y}(f_1,f_2) = \frac{1}{K}\sum_{k=0}^{K-1} x_k(f_1)y_k^{(*)}(f_2). \tag{32}$$

This is recognizable as a dual-frequency cross-spectrum. As before, one can normalize the Loève spectrum to obtain the Loève coherence defined as follows

$$\hat{c}_{x,y}(f_1,f_2) = \frac{|S_{x,y}(f_1,f_2)|^2}{S_{x,x}(f_1)S_{y,y}(f_2)} \tag{33}$$

where $S_{x,x}(f_1)$ and $S_{y,y}(f_2)$ are multitaper estimates of the spectrum (31) using uniform weighting.

Estimation of the Loève spectrum using a periodogram technique is discussed in [20, p 223]. This dual frequency estimator suffers from the same deficiency as the ordinary periodogram, that is, the estimator is asymptotically unbiased but is inconsistent; its variance does not vanish as $N \to \infty$. In general the sampling distributions for dual frequency spectra and coherences are the same as those for ordinary spectra and coherences [28], so the χ^2_{2K-2} distribution of multitaper spectrum estimates is carried over to multitaper dual frequency spectra [27]. That is, for fixed bandwidth, the multitaper Loève dual frequency spectrum is consistent.

References

[1] G. E. P. Box and G. M. Jenkins. *Time Series Analysis: Forecasting and Control*. Holden-Day, San Francisco, 1970.

[2] D. R. Brillinger. *Time Series, Data Analysis and Theory*. Holt, Rinehart, and Winston, New York, 1975.

[3] C. Chatfield. *The Analysis of Time Series, an Introduction*. Chapman and Hall/CRC press, Boca Raton, FL, USA, 6th edition, 2004.

[4] C. W. Chow, B. Urquhart, M. Lave, A. Dominguez, J. Kleissl, J. Shields, and B. Washom. Intra–hour forecasting with a total sky imager at the UC San Diego solar energy testbed. *Solar Energy*, 85(11):2881–2893, 2011.

[5] H. Cramér. On the theory of stationary random processes. *Ann. of Math.*, 41:215–230, 1940.

[6] A. V. Dandawate and G. B. Giannakis. Asymptotic theory of mixed time averages and kth-order cyclic-moment and cumulant statistics. *Information Theory, IEEE Transactions on*, 41(1):216–232, 1995.

[7] W. A. Gardner. *Statistical spectral analysis: a nonprobabilistic theory*. Prentice-Hall, Inc., 1986.

[8] W. A Gardner. An introduction to cyclostationary signals. *Cyclostationarity in communications and signal processing*, pages 1–90, 1994.

[9] W. A. Gardner, A. Napolitano, and L. Paura. Cyclostationarity: Half a century of research. *Signal processing*, 86(4):639–697, 2006.

[10] H. L. Hurd and A. Miamee. *Periodically Correlated Random Sequences*. John Wiley and Sons, New York, 2007.

[11] T. Katayama and S. Sugimoto. *Statistical Methods in Control & Signal Processing*. CRC Press, 1997.

[12] J. Kleissl. *Solar energy forecasting and resource assessment*. Academic Press, 2013.

[13] G. Kopp and J. L. Lean. A new, lower value of total solar irradiance: Evidence and climate significance. *Geophysical Research Letters*, 38(1), 2011.

[14] J. M. Lees and J. Park. Multiple-taper spectral analysis: A stand-alone C-subroutine. *Computers & Geosciences*, 21(2):199–236, 1995.

[15] K. Q. Lepage and D. J. Thomson. Spectral analysis of cyclostationary time–series: A robust method. *Geophys. J. Inter.*, 179:1199–1212, 2009.

[16] M. Loève. *Probability Theory*. D. Van Nostrand, Princeton, NJ, 1963.

[17] D. C. McLernon. Parametric modelling of cyclostationary processes. *International journal of electronics*, 72(3):383–399, 1992.

[18] R. Mellors, F. L. Vernon, and D. J. Thomson. Detection of dispersive signals using multitaper double frequency coherence. *Geophys. J. Inter.*, 135:146–154, 1998.

[19] D. Middleton. *Statistical Communication Theory*. McGraw-Hill, New York, 1960.

[20] A. Napolitano. *Generalizations of cyclostationary signal processing: spectral analysis and applications*, volume 95. John Wiley & Sons, 2012.

[21] D. B. Percival and A. T. Walden. *Spectral Analysis for Physical Applications: Multitaper and Conventional Univariate Techniques*. Cambridge Univ. Press, Cambridge, 1993.

[22] G. A. Prieto, R. L. Parker, and F. L. Vernon III. A fortran 90 library for multitaper spectrum analysis. *Computers & Geosciences*, 35(8):1701–1710, 2009.

[23] H. Sakai and S. Ohno. Theory of cyclostationary processes and its applications. *Statistical Methods in Control and Signal Processing*, pages 327–354, 1997.

[24] D. Slepian. Prolate spheroidal wave functions, Fourier analysis, and uncertainty V: the discrete case. *Bell System Tech. J.*, 57:1371–1429, 1978.

[25] D. J. Thomson. Spectrum estimation and harmonic analysis. *Proceedings of the IEEE*, 70:1055–1096, 1982.

[26] D. J. Thomson. Quadratic-inverse spectrum estimates: applications to paleoclimatology. *Phil. Trans. R. Soc. Lond. A*, 332:539–597, 1990.

[27] D. J. Thomson. Multitaper analysis of nonstationary and nonlinear time series data. In W. Fitzgerald, R. Smith, A. Walden, and P. Young, editors, *Nonlinear and Nonstationary Signal Processing*, pages 317–394. Cambridge Univ. Press, Cambridge, 2001.

[28] D. J. Thomson. Some problems in the analysis of possibly cyclostationary data. In *Proc. Forty–Fifth Asilomar Conf. on Signals, Systems, and Computers*, pages 2040–2044. IEEE, 2011.